Interference effects in acoustic-phonon Raman scattering from GaAs/AlAs mirror-plane superlattices

M. Giehler

Max-Planck-Institut für Festkörperforschung, Heisenbergstrasse 1, D-70569 Stuttgart, Germany
and Paul-Drude-Institut für Festkörperelektronik, Hausvogteiplatz 5-7, D-10117 Berlin, Germany

T. Ruf and M. Cardona

Max-Planck-Institut für Festkörperforschung, Heisenbergstrasse 1, D-70569 Stuttgart, Germany

K. Ploog

Paul-Drude-Institut für Festkörperelektronik, Hausvogteiplatz 5-7, D-10117 Berlin, Germany

Raman scattering of longitudinal-acoustic phonons has been studied in finite-size mirror-plane superlattices (MPSL's) with building blocks $SL=$(GaAs)$_{13}$/(AlAs)$_{18}$ and $LS=$(AlAs)$_{18}$/(GaAs)$_{13}$, arranged to form layer sequences $(SL)_{m/2}/(LS)_{m/2}$ with different numbers of building blocks m. In contrast to periodic structures $(SL)_m$, the folded LA-phonon doublets in MPSL's experience pronounced splittings, while satellites appear around the main lines. These effects are due to the interference of the scattering contributions from the different quantum wells in the sample, and reflect a phase shift introduced by the mirror-plane symmetry. This phase shift can be tuned by GaAs buffers of different widths in structures of the type $(SL)_{m/2}/$ $(GaAs)_n/(LS)_{m/2}$. [S0163-1829(97)05711-1]

I. INTRODUCTION

In an *ideal* periodic superlattice consisting of an infinite sequence of building blocks AB made of different semiconductors A and B, the branches of the acoustic-phonon dispersion are backfolded and quasicontinuous due to the large number of atoms involved. In Raman processes involving longitudinal-acoustic (LA) phonons in backscattering geometry along the growth direction ($\hat{z}$), crystal momentum is conserved almost exactly, i.e., the wave vector q_z transferred to the phonon corresponds to the sum of the magnitudes of the wave vectors for incident and scattered photons k_l and k_s, respectively. Characteristic doublets are observed in the spectrum which reflect the backfolded superlattice dispersion.[1,2] Crystal-momentum conservation at the doublet frequencies implies that all partial waves are coherently scattered, e.g., all GaAs layers of a GaAs/AlAs superlattice contribute constructively to the total intensity. Therefore, the doublets are very sharp and pronounced.

In a *real* superlattice the coherence of the scattering contributions from the individual wells is partly removed due to interface roughness and layer thickness fluctuations. This yields an incoherent contribution to the Raman signal which causes a continuous emission background and is very strong under resonant excitation.[3–7] Under such circumstances crystal-momentum conservation is relaxed to a certain degree and features of the phonon density of states may be observed.[6,7] Interface broadening, e.g., by thermal treatment which does not change the periodicity, only decreases the intensity of the folded-phonon doublets while their widths and positions remain largely unaffected.[1] On the other hand, layer thickness fluctuations lead to additional periodicities. Doublet fine structure in the Raman spectra of Si/Si$_{1-x}$Ge$_x$

superlattices has been attributed to these effects and exploited to establish a method of structural sample characterization.[8,9] Recently, the effect of different length scales has been further investigated in Si/Ge microstructures deliberately grown with two different periodicities.[10]

Crystal-momentum conservation is also relaxed in finite-size superlattices with only a few periods. Raman spectra of Si/Si$_{1-x}$Ge$_x$ structures thus show weak satellites around the main folded-phonon doublet peaks which originate from standing waves of the whole superlattice.[8,9] As far as light scattering is concerned, this effect is analogous to a multislit diffraction experiment with the satellites corresponding to the side maxima. Consequently, their intensity rapidly vanishes away from the main doublets. In GaAs/AlAs superlattices this effect is much harder to observe since the sound velocity, and thus the mode spacing, is only half as large as in Si/Si$_{1-x}$Ge$_x$.[9]

In this paper we report an interesting approach to investigate finite-size effects and the coherence properties of Raman scattering by acoustic phonons in GaAs/AlAs structures. This is possible in samples with built-in phase shifts consisting, e.g., of two building blocks which are denoted by $SL=$(GaAs)$_n$/(AlAs)$_{n'}$ and $LS=$(AlAs)$_{n'}$/(GaAs)$_n$ in the following. Stacking two of these entities in the form $(SL)_{m/2}/(LS)_{m/2}$ leads to mirror-plane superlattices (MPSL's) with the total number of blocks m. Further degrees of freedom arise when buffer (cavity) layers of different thickness are introduced between the SL and LS components.

II. EXPERIMENT

MPSL's with nominal building blocks $SL = $(GaAs)$_{13}$/(AlAs)$_{18}$ and $LS=$(AlAs)$_{18}$/(GaAs)$_{13}$ were grown by
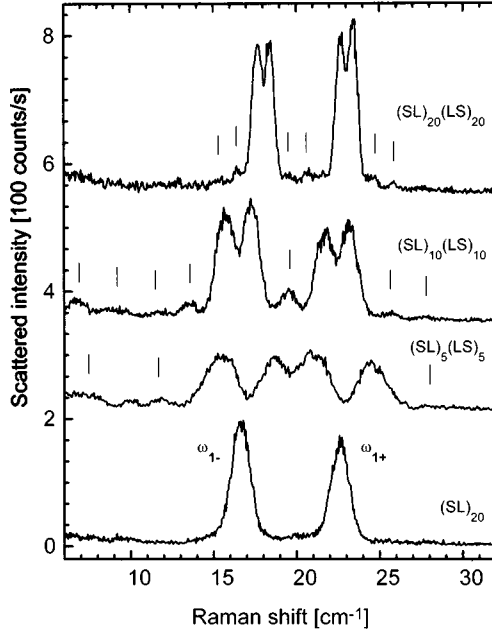
FIG. 1. LA-phonon Raman spectra of $(SL)_{m/2}/(LS)_{m/2}$ MPSL's with $m = 10$, 20, and 40 compared with that of the ideal finite-size structure $(SL)_{20}$. The building blocks are $SL = (GaAs)_{13}/(AlAs)_{18}$ and $LS = (AlAs)_{18}/(GaAs)_{13}$ (in ML), respectively. Minor lines are marked by vertical bars.

molecular-beam epitaxy on [001]-oriented GaAs substrates. The relative layer thicknesses were chosen to obtain a close-to-maximum first-zone-edge dispersion gap around 10 cm^{-1} which is easily accessible with most Raman spectrometers.[2] High-resolution x-ray-diffraction measurements yield actual layer thicknesses of $d_{GaAs} = 13.55$ ML and $d_{AlAs} = 17.65$ ML, with a variation from sample to sample better than ± 0.25 ML. We investigated $(SL)_{m/2}/(LS)_{m/2}$ samples with $m = 10$, 20, and 40 as well as a reference specimen $(SL)_{20}$. Measurements on MPSL's containing buffers were done on $(SL)_{10}/(GaAs)_n/(LS)_{10}$ structures with $n = 9$, 18, 36, and 45. Raman spectra were recorded with the samples at room temperature using a Spex 1404 double monochromator with a cooled GaAs photomultiplier and conventional single-photon-counting electronics. The spectral resolution, as determined from measurements of the laser line, was set to about 0.4 cm^{-1}. The spectra were excited with the 457.9-nm line of an Ar-ion laser using an average power of 250 mW focused to a point about 50 μm diameter. Care was taken to avoid effects due to sample heating. The experiments were performed in near-backscattering geometry. We used parallel polarizations of exciting and detected light along the [001] axis.

III. RESULTS AND DISCUSSION

A. Interference effects in MPSL's

Figure 1 shows Raman spectra of three MPSL's and the $(SL)_{20}$ reference sample in the frequency range of the first LA-phonon doublet. For the reference sample the crystal-momentum transfer $q_z = k_l + k_s = 4\pi n/\lambda$ is about 0.3 π/d_0, where n is the average refractive index and $d_0 = 31$ ML is the superlattice period. One therefore observes a folded-phonon

doublet close to the center of the superlattice Brillouin zone whose components are denoted by $\omega_{1\pm}$. The spectra of the MPSL's display pronounced splittings of the doublet lines. These splittings increase with decreasing total length of the SL and LS building blocks. Furthermore, additional minor lines (marked by vertical bars) with characteristic separations appear.

In the following we present a theoretical model for acoustic-phonon Raman scattering in finite-size MPSL's, and compare it with the experimental results. Assuming photoelastic scattering the Raman intensity is proportional to[1,11]

$$I(\omega_{q_z}) \sim \frac{1}{\omega_{q_z}} \left[n(\omega_{q_z}) + \frac{1}{2} \pm \frac{1}{2} \right] \left| \int dz \ e^{i(k_1 + k_s)z} p(z) \frac{\partial u(z)}{\partial z} \right|^2. \tag{3.1}$$

The integration over exponentials for an infinite superlattice leads to crystal-momentum conservation, and doublet peaks are observed at wave vectors $q_z = k_l + k_s$. In Eq. (3.1) $p(z)$ is the spatially varying photoelastic constant, $u(z)$ the phonon displacement, and $n(\omega_{q_z})$ the Bose-Einstein statistical factor. The plus and minus signs hold for Stokes and anti-Stokes scattering, respectively. The derivative $\partial u(z)/\partial z$ is the ϵ_{zz} component of the strain caused by a LA phonon propagating along $\hat{z}$. We further assume that the light propagates in the MPSL like in a homogeneous medium.

From the observation of equidistant minor lines in the spectra of the MPSL's shown in Fig. 1, we conclude that the relevant $u(z)$ are standing waves of the whole structure along the growth direction. We thus take

$$u(z) = \cos(q_z z), \quad q_z = \pi l/D,$$

$$\omega_{q_z} = |q_z| v_{ac} \quad (l = \pm 1, \pm 2, \pm 3, \dots). \tag{3.2}$$

The total length of the MPSL is $D = m(d_{GaAs} + d_{AlAs})$. The average sound velocity in the MPSL is approximated by that of an ideal superlattice, i.e., $v_{ac} = (d_{GaAs} v_{GaAs} + d_{AlAs} v_{AlAs})/(d_{GaAs} + d_{AlAs})$, v_{GaAs} and v_{AlAs} being the velocities of LA phonons in the two constituent materials.[1,11] The integration in Eq. (3.1) has to be carried out over the MPSL. In Eq. (3.2) we have assumed that the strain vanishes at both ends of the MPSL. We also use a linear dispersion which is valid in the superlattice Brillouin zone away from the edges where gaps occur. For the specific relative layer thickness chosen here, this approximation holds even at the zone center since the dispersion gaps there almost vanish.[2] The assumption of slablike LA phonons localized within the MPSL is somewhat artificial. We therefore also consider mode penetration into the underlying GaAs. For thick substrates the phonon wave vector then becomes quasicontinuous, i.e., q_z and ω_{q_z} in Eq. (3.2) can take arbitrary values.

In order to obtain a better understanding of the interference effects we have integrated Eq. (3.1) analytically using Eq. (3.2). By taking $d_{GaAs} = d_{AlAs} = d/2$, where $d = d_{GaAs} + d_{AlAs}$, we avoid tedious summations over different exponentials and a loss of physical insight. However, this does not affect the mirror-plane symmetry of the system and the interference effects. With this approximation we obtain the following equation for the Raman intensity of a $(SL)_{m/2}/(LS)_{m/2}$ structure
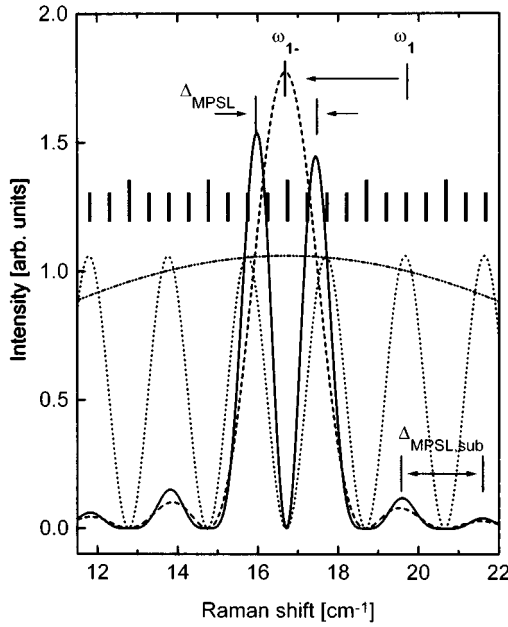
FIG. 2. Calculated Raman spectrum around the lower-energy folded-phonon doublet ω_{1-} in a $(SL)_{10}/(LS)_{10}$ structure (building blocks as in Fig. 1). Solid line: total intensity [Eq. (3.3)]; dashed, dash-double dotted, and dotted lines indicate the squared magnitudes of the contributions from Eqs. (3.4), (3.5), and (3.6), respectively. Due to interference effects the ω_{1-} line is split in two lines separated by Δ_{MPSL}. The various contributions are normalized differently. The frequencies of the discrete eigenmodes of the whole structure according to Eq. (3.2) are given by the vertical bars. See text for details.

$$I(\omega_{q_z}) \sim |A(k+q_z)B(k+q_z)C(k+q_z)$$
$$+ A(k-q_z)B(k-q_z)C(k-q_z)|^2, \quad (3.3)$$

with

$$A(k \pm q_z) = q_z \sum_{r=1}^{m/2} \frac{e^{i(k \pm q_z)rd}}{k \pm q_z}, \quad (3.4)$$

$$B(k \pm q_z) = e^{-i(k \pm q_z)(d/2)} - 1, \quad (3.5)$$

$$C(k \pm q_z) = \pm (p_{GaAs} - p_{AlAs})[1 - e^{i(k \pm q_z)(m/2)d}], \quad (3.6)$$

and $k = k_l + k_s = 4\pi n/\lambda$. Due to the small phonon energies involved $k_l + k_s$ can be approximated by $2k_l$. A fixed value of k is thus determined by the exciting laser wavelength used in an experiment. The values of q_z are determined by Eq. (3.2) and the phonon energy where $I(\omega_{q_z})$ is evaluated. Figure 2 displays the Raman spectrum calculated according to Eq. (3.3) (solid line) and the squared magnitudes of the three individual terms of Eqs. (3.4)–(3.6) (dashed, dashed-double dotted, and dotted lines, respectively) for a $(SL)_{10}/(LS)_{10}$ structure. For clarity we only consider effects on the lower-energy component ω_{1-} of the folded-phonon doublet in the following, i.e., terms depending on $k - q_z$ in Eq. (3.3) are neglected. The spectra were computed with $v_{GaAs} = 4.71 \times 10^5$ cm/s, $v_{AlAs} = 5.65 \times 10^5$ cm/s,[11] $p_{GaAs} = 40.7 + 199.1i$, and $p_{AlAs} = 28.3$.[12] For the average refractive index we used $n = 3.9$ for 458 nm excitation.[13] For the building block thick-

ness we took $d = 31.4$ ML. The vertical bars in Fig. 2 denote the frequencies of the standing waves according to Eq. (3.2) for a superlattice or MPSL with 20 building blocks.

Equation (3.4) (the dashed line in Fig. 2) represents the conservation of crystal momentum which is exact for $m \to \infty$. However, due to the finite size of the structure we do not obtain a δ-like peak for the low-frequency doublet component ω_{1-} but a maximum with nonvanishing width and several side peaks. As can be seen by a comparison of the dashed line with the vertical bars in Fig. 2, the scattering intensity of a folded-phonon doublet peak does not arise only from one model, but from several modes. For the average frequency of the folded-phonon doublets $\omega_s = (\omega_{s+} + \omega_{s-})/2$ (corresponding to $k = 0$) we directly obtain, using Eq. (3.4), the well-known relation $\omega_s = 2s\omega_{Bragg1}$, where $\omega_{Bragg1} = v_{ac}\pi/d$, and $s = 0,1,2 \ldots$ is the index of the zone-center doublet. The frequency splitting of the doublet lines (for $k \neq 0$) is $\Delta_{\pm} = \pm (q_z d/\pi)\omega_{Bragg1}$, hence the doublet frequencies of the ideal structure, are $\omega_{s\pm} = \omega_s + \Delta_{\pm}$. For the mode index l_s of the standing sound wave at the average doublet frequency ω_s Eq. (3.4) gives $l_s = 2sm$. For the $(SL)_{10}/(LS)_{10}$ structure, we obtain $\omega_1 = 19.7$ cm^{-1}, $l_1 = 40$, and $\Delta_{\pm} = \pm 3$ cm^{-1}. For a periodic $(SL)_m$ structure Eq. (3.4) has the same form except that the summation extends up to m. Therefore, the doublet frequencies are the same for a $(SL)_{m/2}/(LS)_{m/2}$ MPSL and a $(SL)_m$ superlattice. However, as we shall discuss below, interference effects lead to a frequency separation between minor lines with nonvanishing Raman intensity in the MPSL which is twice as large as in a superlattice with identical total thickness.

The contribution of Eq. (3.5) to the doublet intensities is a slowly varying function of frequency as shown by the dashed-double dotted line in Fig. 2. Equation (3.5) has the same form for MPSL's and SL's. It is responsible for the vanishing intensity of the even-s folded-phonon doublets in samples where $d_{GaAs} \simeq d_{AlAs}$.[2]

The first term of Eq. (3.6) is the same for SL's and MPSL's. Due to its presence the contribution of all GaAs wells to the scattered field is partly compensated for the contributions of all AlAs wells, and scattering arises only from the modulation of the photoelastic constants. For a homogeneous material the folded-phonon doublets thus disappear. The second term in Eq. (3.6) describes the interference effect of the scattered field from the $(LS)_{m/2}$ unit with that of the $(SL)_{m/2}$ building block. It has a strongly oscillatory behavior (see the dotted lines in Fig. 2). The most dramatic consequence of this term is the vanishing intensity of the folded-phonon doublet component at ω_{1-} and its splitting into two separate lines. At $k = 0$ we obtain $\omega_{\bar{s}} = (4\bar{s}/m)\omega_{Bragg1}$ for the frequencies where Eq. (3.6) becomes zero ($\bar{s} = 0,1,2 \ldots$ is the index of the minimum). The comparison with Eq. (3.2) yields $l = 4\bar{s}$. This means that the intensity of every fourth standing wave in a MPSL is suppressed by interference effects due to the mirror-plane symmetry. The frequencies of these modes are indicated by the longer vertical bars in Fig. 2. For $k \neq 0$ the minima of Eq. (3.6) shift by $\Delta_{\pm} = \pm (q_z d/\pi)\omega_{Bragg1}$, i.e., by the same amount as the doublet lines. Therefore, Eq. (3.6) becomes zero at the frequencies of the doublet lines $\omega_s + \Delta_{\pm}$, independent of the value of k transferred in the scattering process. At the folded-phonon doublets the contribution of the $(SL)_{m/2}$ building

block is thus completely canceled by the contribution of the $(LS)_{m/2}$ unit, i.e., the coherent contributions to the Raman signal of both building blocks in a MPSL have the same magnitude but a phase shift of π. The total scattering intensity in the MPSL (solid line in Fig. 2) thus vanishes at frequencies where the ideal superlattice has folded-phonon doublet peaks. In the Raman spectra of MPSL's the superlattice folded-phonon doublets are therefore split into two components, respectively. However, the positions of the weaker side peaks, which have nonvanishing intensities due to finite-size effects (see above), remain almost unaffected. As can be seen in Fig. 2, the modulation due to Eq. (3.6) (dotted line), is now in phase with the side maxima given by Eq. (3.4) (dashed line), and constructive interference occurs. This leads to an enhancement of their scattering intensity which facilitates the experimental observation. Note that the frequency separation between the split main lines is not exactly equal to $4\omega_{\text{Bragg1}}/m$, as demonstrated by the dotted line in Fig. 2. Due to the strong contribution of Eq. (3.4) (dashed line in Fig. 2) the product of all three terms in Eq. (3.3) for the Raman intensity reduces the splitting to an effective value of $\Delta_{\text{MP}SL} \simeq 3\omega_{\text{Bragg1}}/m$. For the minor lines, however, the influence of Eq. (3.4) is small, and therefore their frequency separation is equal to that expected from Eq. (3.6), i.e., $\Delta_{\text{MP}SL,\text{sub}} = 4\omega_{\text{Bragg1}}/m$. For a $(SL)_{10}/(LS)_{10}$ MPSL we thus calculate for the frequency separation of the main lines $\Delta_{\text{MP}SL} = 1.5$ and for the minor lines $\Delta_{\text{MP}SL,\text{sub}} = 2$ cm^{-1}. For a $(SL)_5/(LS)_5$ [$(SL)_{20}/(LS)_{20}$] structure we obtain $\Delta_{\text{MP}SL} = 3$ cm^{-1} (0.74 cm^{-1}) and $\Delta_{\text{MP}SL,\text{sub}} = 3.9$ cm^{-1} (1.0 cm^{-1}). Note that the calculations in Fig. 2 will be modified slightly due to the interference of the $(k+q_z)$ and $(k-q_z)$ terms in Eq. (3.3), which has been neglected so far. However, the frequency splittings are not affected.

We now compare our theoretical and experimental results. Figure 3 shows Raman spectra calculated by integrating Eq. (3.1). The thickness d of a $(\text{GaAs})_{13}/(\text{AlAs})_{18}$ unit has been used as a fitting parameter. In deriving individual layer thicknesses from the values of d obtained by the fits, we used the relation $d_{\text{GaAs}}/d_{\text{AlAs}} \approx v_{\text{GaAs}}/v_{\text{AlAs}}$, which holds for samples which maximize the first-zone-edge gap such as those considered here. For the samples $(SL)_{20}$ and $(SL)_m/(LS)_m$ with $m = 5$, 10, and 20, we obtain values of $d = 31.4$, 30.2, 31.7, and 30.0 ML, respectively, in agreement with the x-ray data. In order to take the finite penetration depth of light into account, we further assume that the amplitude of the electric field decreases to $1/e$ over a distance of $2D((SL)_{20})$ corresponding to an average absorption coefficient of about 2.8×10^4 cm^{-1}.

The results of calculations assuming discrete confined slab modes of the whole structure in Eq. (3.2) are shown in Fig. 3 as vertical lines. The results assuming mode penetration into the substrate, i.e., allowing for continuous values of q_z and ω_{q_z} are given by solid lines. Both types of spectra display essentially the same behavior. Therefore it is not the effect of mode confinement in the MPSL or superlattice which is important but that of coherence, i.e., the interference of the scattering contributions from different parts of the structures.
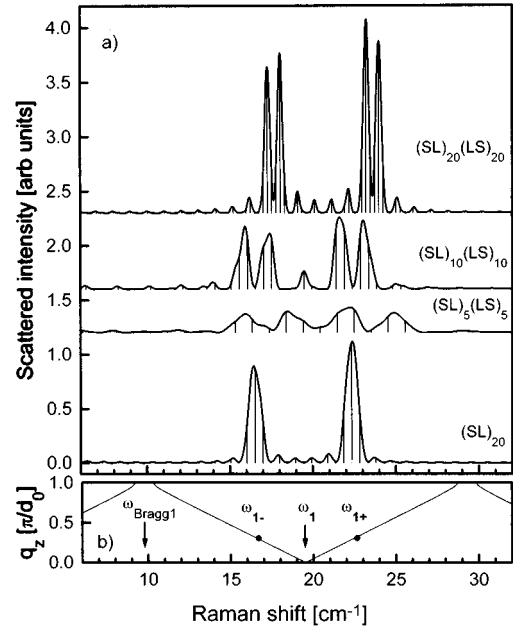
FIG. 3. (a) Raman spectra calculated numerically according to Eq. (3.1) for the samples of Fig. 1. The vertical bars give the scattering intensities of the discrete eigenmodes of the whole structures. The solid lines were calculated under the assumption of a continuous mode spectrum. (b) Modes observed for $(SL)_{20}$ (dots) in comparison with the LA-phonon superlattice dispersion.

Comparing Figs. 1 and 3, we find rather good agreement between the measured and calculated Raman spectra. From the calculations we obtain for the frequency splittings values of $\Delta\omega_{\text{MP}SL} = 2.6$, 1.5, and 0.8 cm^{-1} for $m = 10$, 20, and 40, respectively. This is in good agreement with the analytically estimated values given above, and the experimentally determined ones of 3.5 ± 0.4, 1.4 ± 0.1, and (0.75 ± 0.1) cm^{-1}. Due to the larger intensity difference between major and adjacent minor lines in $(SL)_{20}$ than in the MPSL's and the smaller frequency separation between minor lines for the same total thickness of the structure, finite-size features in periodic GaAs/AlAs superlattices cannot be clearly identified experimentally, as was already pointed out in Ref. 9. They are, however, quite prominent in MPSL's where scattering is modified by interference effects.

The linewidths of the peaks in Fig. 1 are determined by the degree of relaxation in crystal-momentum conservation due to finite-size effects and by the spectral resolution. The determination of the intrinsic phonon linewidth due to anharmonic interactions requires higher-resolution measurements which are in progress.

A complete cancellation of the folded-phonon doublet intensities ($\omega_{1\pm}$) occours only if the scattering contributions of the first and second building blocks of the MPSL have the same magnitude and a phase shift of π. However, if the light is attenuated within the MPSL, the scattered intensity does not go to zero at $\omega_{1\pm}$. In order to obtain a complete cancellation, the mirror plane should be shifted from the center toward the front side of the sample, depending on the penetration depth of the light. Zero intensity might thus be achieved, e.g., in $(SL)_n/(LS)_m$ samples with $n < m$.
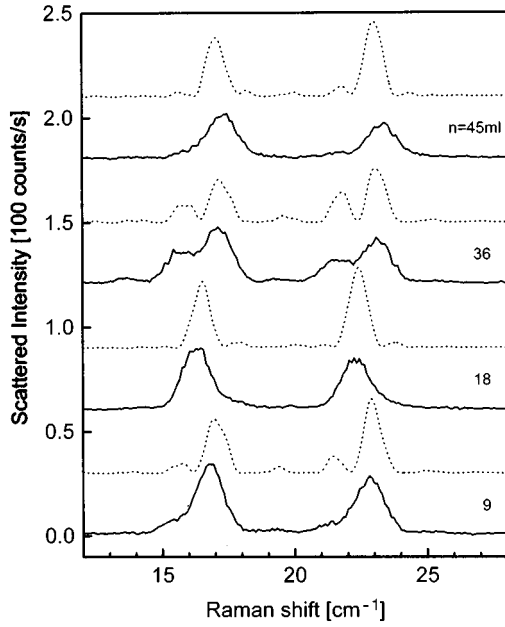
FIG. 4. Measured (solid lines) and calculated (dotted lines) Raman spectra of buffer layer MPSLs $(SL)_{10}/(GaAs)_n/(LS)_{10}$ for different values of n in ML.

B. MPSL's with a buffer layer

The phase shift between the two MPSL building blocks can be modified by the introduction of a buffer layer into the center of a sample. For a $(SL)_{m/2}/(GaAs)_n/(LS)_{m/2}$ system, this leads to a modification of Eq. (3.6), which has to be replaced by

$$C(k \pm q_z) = \pm (p_{GaAs} - p_{AlAs})[1 - e^{i(k \pm q_z)d_{cav}} e^{i(k \pm q_z)(m/2)d}],$$
$$(3.7)$$

where d_{cav} is the thickness of the $(GaAs)_n$ buffer layer. The effect of the buffer layer on the phase difference between the waves scattered by the $(SL)_{m/2}$ and $(LS)_{m/2}$ building blocks is described by the additional phase factor $e^{i(k \pm q_z)d_{cav}}$. For increasing buffer layer thickness the period of the oscillations in Eq. (3.7) decreases and, depending on the specific value of d_{cav}, the interference between the two superlattice blocks at the folded-phonon frequency $\omega_{1\pm}$ can be continuously tuned from fully constructive (periodic superlattice with unsplit folded-phonon lines) to destructive (MPSL with split lines). Figure 4 shows measured (solid lines) and calculated Raman spectra [dashed lines, Eq. (3.1)] of such cavity structures with GaAs buffers between $(SL)_{10}$ and $(LS)_{10}$ building blocks.

For the sample with $d_{cav}=9$ ML, the reduction in the period of the term given by Eq. (3.7) causes a shift of the MPSL peaks at $\omega_{1\pm} \pm \Delta_{MPSL}/2$ toward lower frequencies. The components at $\omega_{1\pm} - \Delta_{MPSL}/2$ therefore have to be multiplied by smaller values of the envelope given by Eq. (3.4) (see the dashed line in Fig. 2) and their intensity decreases. For the peaks at $\omega_{1\pm} + \Delta_{MPSL}/2$ the factor from Eq. (3.4) increases, and the Raman signal becomes stronger. This

leads to the strongly asymmetric calculated doublets shown in Fig. 4, which are in good agreement with the experimental results.

For $d_{cav}=d/2$ the $(SL)_{m/2}/(GaAs)_n/(LS)_{m/2}$ structure can be approximated by a $(SL)_{m+1}$ superlattice. At $\omega_{1\pm}$ all GaAs quantum wells contribute constructively to the interference. This case is realized for the sample with $d_{cav}=18$ ML in Fig. 4 which displays only unsplit folded-phonon doublets. Compared to the $(SL)_{20}$ spectrum in Fig. 3, however, the peaks are shifted toward lower frequencies because d_{cav} exceeds the width of the other GaAs quantum wells in this sample (13 ML) by a few monolayers.

When $d_{cav}=d$, Eq. (3.7) is the same as Eq. (3.6) for a system with two more periods (i.e., $m \to m+2$). We therefore expect effects similar to those in MPSL's without a buffer. This can be seen by comparing the spectrum for the sample with $d_{cav}=36$ ML in Fig. 4 with the curve for $(SL)_{10}(LS)_{10}$ in Fig. 3. The asymmetry of the split-line intensities arises from d_{cav} being slightly larger than $d \simeq 31$ ML in this sample.

With increasing buffer thickness the alternation between unsplit and split phonon doublets repeats itself periodically due to the extra factor in Eq. (3.7). The spectrum for $d_{cav}=45$ ML in Fig. 4 is rather similar to the one for $d_{cav}=9$ ML, since the cavity lengths differ by about one period. For large cavity lengths ($d_{cav} \gg d$), however, this additional modulation introduces new zeros in the Raman intensity and we expect further splittings to appear.

MPSL's are systems where interference effects of different contributions to the Raman intensity can be conveniently studied. However, mirror-plane symmetry is not a prerequisite for these effects to occur. We expect similar effects for any layer sequence with artificially introduced phase shifts. As illustrated here for the case of finite-size effects in MPSL's, controlling the phase in Raman processes opens ways to investigate phenomena which are otherwise hardly accessible. These effects should also be useful for the characterization of microcavity lasers where active layers are embedded in Bragg mirrors consisting of superlattices.

IV. CONCLUSIONS

We studied interference effects in the acoustic-phonon Raman spectra of MPSL's which arise from phase shifts between the contributions of different layers to the scattering intensity. This allowed us to investigate finite-size effects which are otherwise hardly accessible. We demonstrated that the interferences and phase shifts can be tuned by the introduction of buffer layers in the center of the MPSL's.

[1] C. Colvard, T. A. Gant, M. V. Klein, R. Merlin, R. Fischer, H. Morkoc, and A.C. Gossard, Phys. Rev. B **31**, 2080 (1985).

[2] B. Jusserand and M. Cardona, in *Light Scattering in Solids V*, edited by M. Cardona and G. Güntherodt (Springer, Heidelberg, 1989), p. 61.

[3] P. S. Kop'ev, D. N. Mirlin, V. F. Sapega, and A. A. Sirenko, Pis'ma Zh. Éksp. Teor. Fiz. **51**, 624 (1990) [JETP Lett. **51**, 708 (1990)].

[4] V. F. Sapega, V. I. Belitsky, T. Ruf, H. D. Fuchs, M. Cardona, and K. Ploog, Phys. Rev. B **46**, 16 005 (1992).

[5] D. N. Mirlin, I. A. Merkulov, V. I. Perel', I. I. Reshina, A. A. Sirenko, and R. Planel, Solid State Commun. **84**, 1093 (1992).

[6] T. Ruf, V. I. Belitsky, J. Spitzer, V. F. Sapega, M. Cardona, and K. Ploog, Phys. Rev. Lett. **71**, 3035 (1993).

[7] T. Ruf, J. Spitzer, V. F. Sapega, V. I. Belitsky, M. Cardona, and K. Ploog, Phys. Rev. B **50**, 1792 (1994).

[8] P. X. Zhang, D. J. Lockwood, H. J. Labbé, and J.-M. Baribeau, Phys. Rev. B **46**, 9881 (1992).

[9] P. X. Zhang, D. J. Lockwood, and J.-M. Baribeau, Can. J. Phys. **70**, 843 (1992).

[10] M. A. Araújo Silva, E. Ribeiro, P. A. Schulz, F. Cerdeira, and J. C. Bean, J. Raman Spectrosc. **27**, 257 (1996).

[11] J. He, B. Djafari-Rouhani, and J. Sapriel, Phys. Rev B **37**, 4086 (1988).

[12] Z. V. Popović, J. Spitzer, T. Ruf, M. Cardona, R. Nötzel, and K. Ploog, Phys. Rev. B **48**, 1659 (1993).

[13] E. D. Palik, *Handbook of Optical Constants of Solids* (Academic, New York, 1985), p. 438.